JOURNAL OF CATALYSIS 139, 48–61 (1993)

Effect of Sulfur on the Performance and on the Particle Size and Location of Platinum in Pt/KL Hexane Aromatization Catalysts

G. B. McVicker,*,[1] J. L. Kao,† J. J. Ziemiak,* W. E. Gates,* J. L. Robbins,* M. M. J. Treacy,* S. B. Rice,* T. H. Vanderspurt,* V. R. Cross,† and A. K. Ghosh*

*Exxon Research and Engineering Company, Corporate Research Science Laboratories, Annandale, New Jersey, 08801; and †Exxon Chemical Company, Basic Chemicals Technology, Baytown, Texas, 77522

Received June 15, 1992; revised August 6, 1992

Sulfur, introduced to a working Pt/KL hexane aromatization catalyst in the form of thiophene, functions as an extremely potent poison by reducing the number of Pt sites accessible within the channels of the KL zeolite. The intrinsic catalytic activity and selectivity of in-channel Pt sites, however, is not significantly modified by the presence of sulfur on the catalyst. Extremely low thiophene feed sulfur concentrations in the 50–200 wppb range accelerate Pt agglomeration. Catalyst deactivation, resulting primarily from metals agglomeration, most likely occurs by multiple blockage of KL channels by small (10–20 Å) Pt and/or Pt–sulfur clusters.

INTRODUCTION

Over the past 10 years numerous researchers have made significant scientific and technological advances in the aromatization of hexane over Pt/KL-zeolite catalyst systems. Notable advances include: identification of process variable and performance relationships much different than those shown by conventional bifunctional reforming catalysts (*1–4*), definition of improved KL-zeolite synthesis and catalyst fabrication chemistries (*5–8*), and development of reliable catalyst regeneration procedures (9, 10).

The sulfur sensitivity of monofunctional Pt/KL hexane aromatization catalysts is qualitatively known to be substantially higher than that of conventional Pt/Cl–Al_2O_3 and Pt–Re/Cl–Al_2O_3 bifunctional reforming catalysts (*11, 12*). Application of the above technological advances is, therefore, dependent to a large extent upon increasing our understanding of, and developing ways of controlling, catalyst deactivation by sulfur. Presently, acceptable Pt/KL aromatization cycle lengths can only be achieved by reducing feed sulfur concentration to ultralow levels (*13*). The subject studies were undertaken to quantify the effect <10 to 200 wppb (weight part per billion) feed sulfur concentrations have on the activity maintenance and selectivity patterns of Pt/KL catalysts. Such information, coupled with detailed Pt structural studies, was anticipated to be useful in clarifying the mechanism by which sulfur, even in trace concentration, so markedly suppresses the performance of Pt/KL catalysts.

EXPERIMENTAL

Catalyst Preparation

Loading 0.6 wt% Pt into bound $\frac{1}{16}$-inch KL extrudate particles was accomplished using an established cation exchange procedure (*14*). Unbound KL powders, also containing 0.6 wt% Pt, were obtained by incipient wetness impregnation using standardized aqueous $[(NH_3)_4Pt]\ Cl_2$ (0.05 g Pt/cm^3) solutions. After drying at 387 K overnight, the Pt-loaded catalysts were activated by air calcination at 623 K. Double

[1] To whom correspondence should be addressed.

0021-9517/93 $5.00

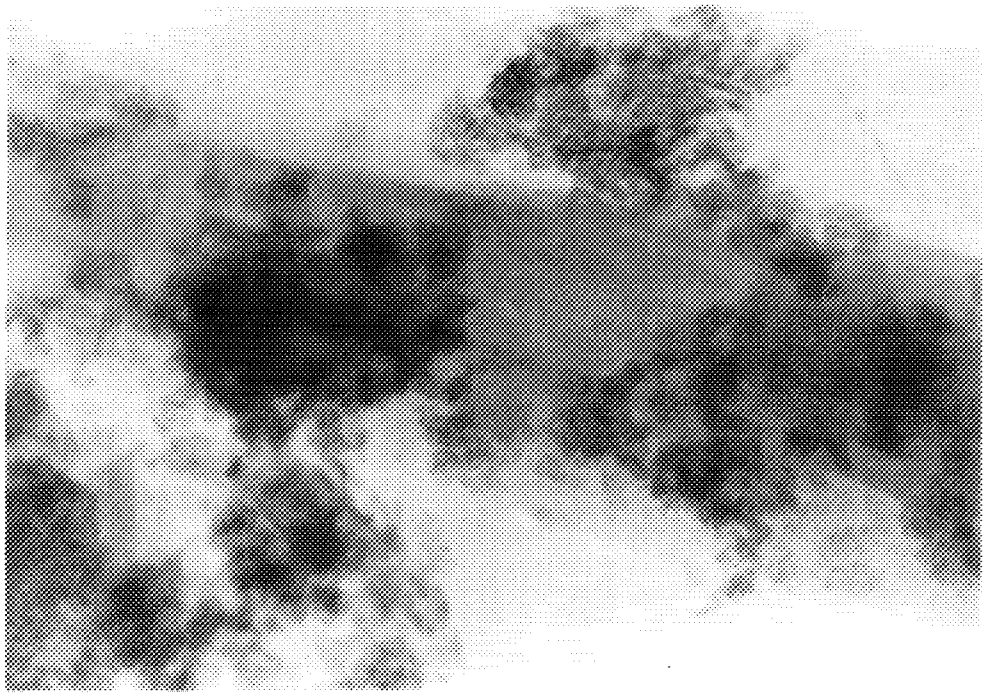

FIG. 1. Bright-field TEM micrograph of a fresh 0.6% Pt/KL extrudate catalyst. KL-zeolite channel spacings (15.9 Å) are visible and provide an internal standard for Pt cluster size measurement.

hydrogen adsorption isotherm measurements (*15*) on fresh catalysts reduced at 773 K typically yield H(irrev)/Pt atom ratios in the 0.9 to 1.1 range, which suggests that the average Pt crystallite size is small, 10 Å or less (*16*). This suggestion is reinforced by bright-field TEM images (see Fig. 1), which routinely show few Pt clusters >10 Å in diameter within the channels of fresh Pt/KL catalysts. Indepth *Z*-contrast STEM studies of fresh Pt/KL catalysts confirmed that most Pt clusters in the KL channels are in fact <10 Å (*vide infra*).

Catalyst Testing

Hexane aromatization reactions were carried out in a 25-cm^3, stainless steel, fixed-bed, isothermal unit operated in a single pass mode. The reactor was heated by a fluidized sand bath. Hydrogen was passed through Deoxo and molecular sieve drying units prior to use. Feed was delivered by a dual-barrel Ruska pump which allowed continuous operation. Aromatization experiments were generally carried out at 783 K under 825 kPa total pressure. Catalysts were reduced *in situ* at 783 K under 825 kPa hydrogen (500 cm^3/min) for 16 hr. Following reduction, the reactor temperature was reduced to 723 K and the hydrogen flow was adjusted to provide an H_2/feed mole ratio of 6.0. Feed was introduced at 723 K and the temperature was increased at 10 K/hr to an operating temperature of 783 K. The starting, nil-sulfur feedstocks contained less than 10 wppb sulfur (*17*). Space velocities, based upon the zeolite component, were varied between 2.5 and 50 WHSV. Direct analyses of all reaction products, methane through the isomeric xylenes, were made by on-line GC measurements. The product train was equipped with a gas phase sparger to insure product homogenization. A 30 ft by $\frac{1}{8}$ inch (o.d.) column packed with 20% SP-2100 al-

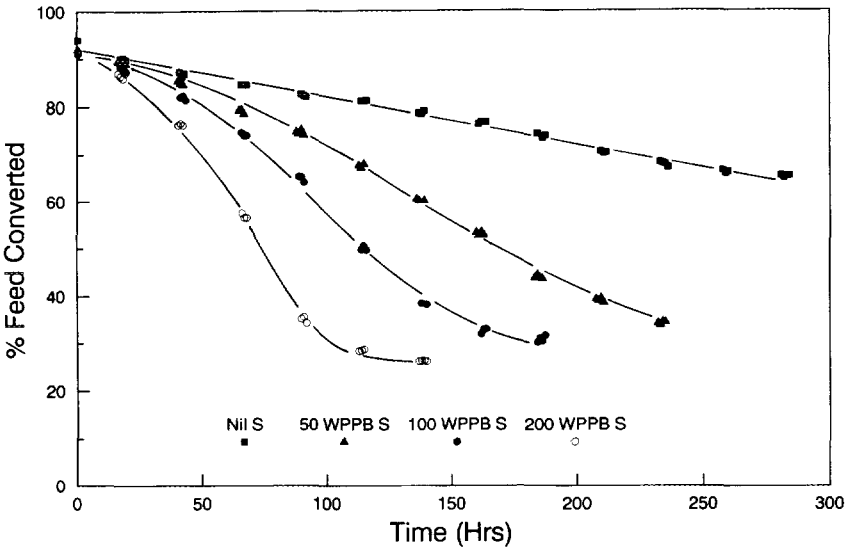

FIG. 2. Feed converted as a function of time and sulfur concentration over a 0.6% Pt/KL extrudate catalyst. Nil-sulfur feed contains no added sulfur; 50–200 wppb sulfur feeds obtained by thiophene addition.

lowed essentially complete product separation and identification. Detection was by flame ionization. Results are reported as wt% feed conversions, wt% benzene yield, and % benzene selectivity, which are defined as

(i) feed conversion (wt%) = 100 − (n-C_6 + MCP)$_f$,

(ii) benzene yield (wt%) = wt% benzene in product,

(iii) benzene selectivity (%) = (wt% benzene/feed conversion) × 100, where n-C_6 and MCP are n-hexane and methylcyclopentane, respectively; f signifies final product compositions.

Feed sulfur adjustments were made using standardized thiophene solutions. A standard 100 wppm (weight part per million) sulfur solution, from which aliquots were withdrawn as needed, was prepared by dissolving 86.6 mg thiophene in 500 cm^3 of n-hexane. This solution was found to contain 108 ± 11 wppm sulfur. Between runs using different feed sulfur levels, the reactor and feed lines were purged with nil-sulfur feed and hydrogen at operating conditions for at least 72 hr.

High-Resolution Electron Microscopy

Investigations of the effect sulfur has on the particle size and distribution of Pt in KL zeolite crystals were carried out using either the transmission electron microscope (TEM) and/or the scanning transmission electron microscope (STEM). Bright-field TEM images were obtained on a Philips 400T FEG operated at 100 kV. High-resolution Z-contrast images of Pt particles were obtained on a VG HB501A STEM, operated at 100 kV and equipped with a high-angle annular dark field detector. For all specimens examined electron beam damage was minimized by using as low an electron dose as practicable. Details of the microscopic techniques and specimen preparation procedures have been reported elsewhere (*18, 19*).

Infrared Spectroscopy

Infrared spectra were recorded on pressed catalyst wafers inside a heatable,

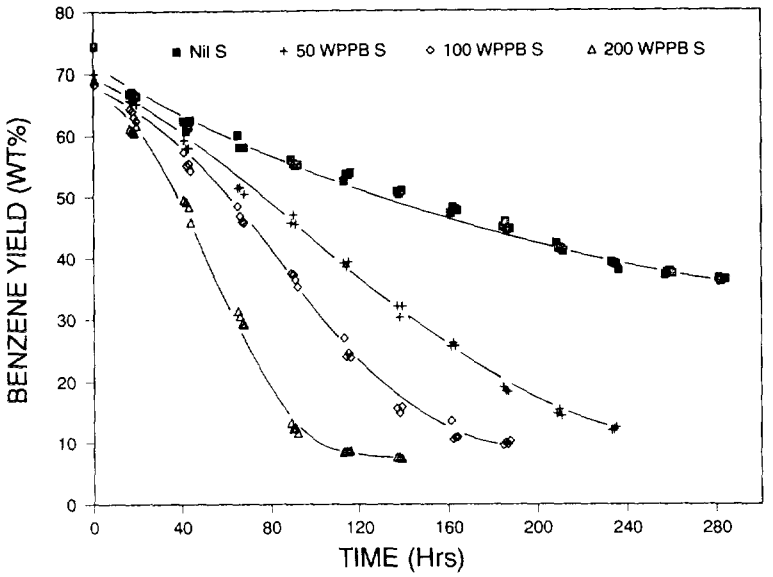

FIG. 3. Benzene yield as a function of time and feed sulfur concentration over a 0.6% Pt/KL extrudate catalyst. Nil-sulfur feed contains no added sulfur; 50–200 wppb sulfur feeds obtained by thiophene addition.

controlled atmosphere IR cell whose design was described previously (*20*). Pt/KL extrudates were ground to a fine powder and pressed into self-supporting 16-mm diameter wafers weighing 35 mg. Both the fresh Pt/KL and a partially deactivated Pt/KL sample were reduced in flowing hydrogen at 673 K for 8 hr prior to preparing the IR wafers. The partially deactivated sample refers to a catalyst discharged from a hexane aromatization experiment after 160 hr of operation under the following conditions: 773 K, 825 kPa total pressure, WHSV = 2.5, 200 wppb sulfur, and an H_2/feed mole ratio of 6.0. Once mounted inside the IR cell, catalyst wafers were heated at 1K/min to 673 K in 10 cm^3/min hydrogen and then held in flowing hydrogen for 2 hr at 673 K. The cell was then evacuated to less than 10^{-6} Torr at 673 K and cooled to 313 K. Background spectra were averaged (16 scans) in the range 2300–1600 cm^{-1} using a ratio-recording grating IR spectrometer (Perkin–Elmer 684). Sample spectra were averaged over the same spectral region after equilibrating the wafer in 10 Torr carbon monoxide for 10 min. The figures shown represent the difference of the sample and background spectra without smoothing. The data are presented in the absorbance format.

RESULTS AND DISCUSSIONS

Effect of Sulfur on the Catalytic Performance of Pt/KL Catalysts

Four separate experiments were conducted to investigate the effect wppb thiophenic sulfur concentrations have upon the performance of Pt/KL catalysts. Reaction conditions were 783K, 825 kPa, 6.6 WHSV, H_2/feed ratio of 6 and a mixed hexane (89%) and methylcyclopentane (11%) feed. Figures 2 through 4 illustrate the time-on-steam behavior of a Pt/KL extrudate catalyst during the aromatization of the mixed C_6 feed both with and without added thiophene. Important performance parameters plotted as a function of time include: feed conversion (Fig. 2), benzene yield (Fig. 3), and benzene selectivity (Fig. 4). In the absence of added sulfur, all three performance parameters de-

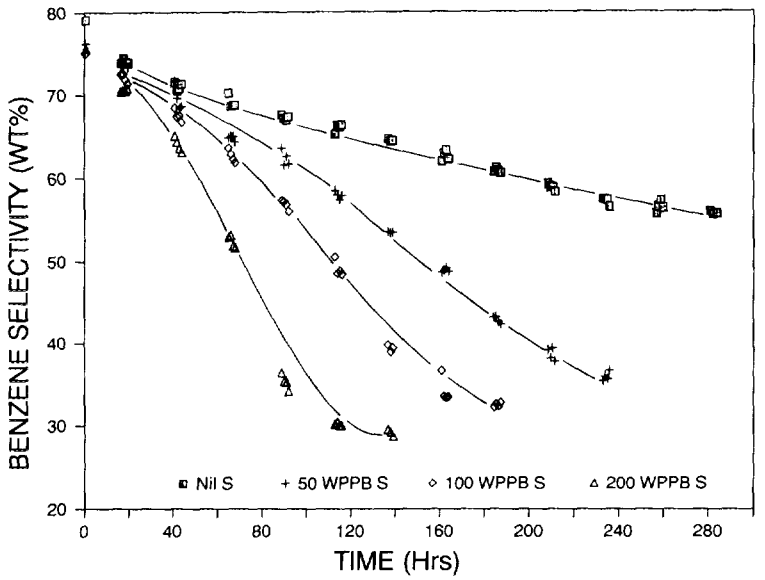

FIG. 4. Benzene selectivity as a function of time and feed sulfur concentration over a 0.6% Pt/KL extrudate catalyst. Nil-sulfur feed contains no added sulfur; 50–200 wppb sulfur feeds obtained by thiophene addition.

clined slowly and nearly linearly throughout the course of a 285-hr run. For the three sulfur-added runs, the corresponding performance parameters declined much more rapidly and with rates of decline dependent upon feed sulfur concentrations. The decline in catalyst productivity with increasing feed sulfur is illustrated in Fig. 5 where the rate of loss of benzene yield (Δ wt%/hr) is shown to be directly proportional to feed sulfur content. The rate of benzene yield loss was determined by measuring the initial, roughly linear, slopes (first 90 hr on feed) of the benzene yield versus time curves shown in Fig. 3.

In the sulfur-added cases the three key performance parameters all tend to stabilize at low, steady-state values. For example, in the run utilizing a 200-wppb sulfur feed the benzene yield does not fall to zero, but converges to a limiting value of about 8% after 125 hr on oil. Similarly, for the 200-wppb sulfur-spiked run benzene selectivity levels out near 30%. Runs using 50 and 100 wppb sulfur feeds also asymptotically approach similar limiting (nonzero) values. It is well known that Pt/KL catalysts exhibit uniquely high hexane aromatization rates and selectivities. This has been attributed in part to collimating effects induced by the unidirectional, narrow tubular KL channel geometry which enforces an end-on approach (or preorganization into a pseudocycle) of *n*-hexane molecules to Pt clusters within the KL channels (*21*, *22*). Initial attachment at the terminal carbon atom would favor dehydrocyclization to benzene (*21*, *23*). Another model posits that high benzene selectivity is a property of clean (coke-free) Pt surfaces (*24*). In this model Pt/KL retains high benzene yields and selectivities with time because the narrow tubular channel geometry inhibits bimolecular coupling reactions leading to coke formation. The above models, as well as electronic promotion models (*25*, *26*), all suggest that high benzene formation rates and selectivities are uniquely associated with Pt particles located within the L zeolite channels. As described above, Pt/KL catalysts rapidly deactivated

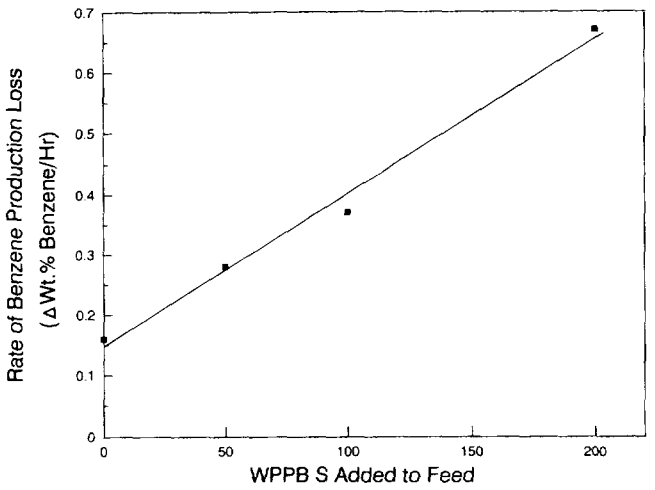

FIG. 5. Effect of feed sulfur content on the rate of loss of benzene yield over of a 0.6% Pt/KL extrudate catalyst. Nil-sulfur feed contains no added sulfur; 50–200 wppb sulfur feeds obtained by thiophene addition.

in sulfur-containing feeds exhibit low, but stable benzene yields and selectivities, reminiscent of those obtained with Pt supported on macroporous, nonacidic supports such as silica. The low and essentially constant benzene yields and selectivities suggest that the residual performance of sulfur-deactivated Pt/KL catalysts reflects the catalytic action of a relatively small number of Pt particles situated outside the influence of the KL channels.

The end-on approach of *n*-hexane toward Pt clusters within the KL channels also favors hydrogenolysis at terminal versus internal carbon–carbon bonds. Thus, for hexane feeds, Pt/KL catalysts typically display unusually high molar ratios of C_5/C_4 hydrogenolysis products when compared to Pt on macroporous supports. This ratio, commonly referred to as the terminal cracking index (*21*) is shown in Fig. 6. Sulfur addition steadily reduces the ability of Pt/KL to selectively rupture the terminal carbon–carbon bond of *n*-hexane. This selectivity modification is consistent with sulfur preferentially reducing the number of Pt sites accessible within the KL channels compared to less selective Pt sites on the exterior surface of the KL crystals.

Further insight into the mechanism by which sulfur deactivates Pt/KL catalysts can be gained by considering the information summarized in Table 1. The times required for benzene yields to converge to limiting values of about 8% were estimated from the benzene yield versus time curves shown in Fig. 3 . By knowing the feed sulfur content, space velocity, and the time required to reach the stable 8% benzene yield plateaus, the quantity of sulfur in terms of S/Pt atom ratio responsible for leveling the benzene yields is easily calculated. At S/Pt atom ratios of about 0.1, the benzene yields of Pt/KL catalysts are consistently reduced to low, but stable steady-state values. Thus, 1 sulfur atom has the apparent ability to deactivate 10 Pt atoms situated within the KL channels. At a Pt loading of 0.6 wt%, approximately 130 Pt atoms can be accommodated within each channel of a KL crystallite 1.2 μm in length, the average length of KL zeolite particles used in this study. If it is assumed that sulfur enhances the rate of formation of Pt agglomerates near the entrance to the KL channels (see Fig. 7), access of a reactant hexane molecule to highly dispersed Pt sites within the KL channel is completely blocked when only

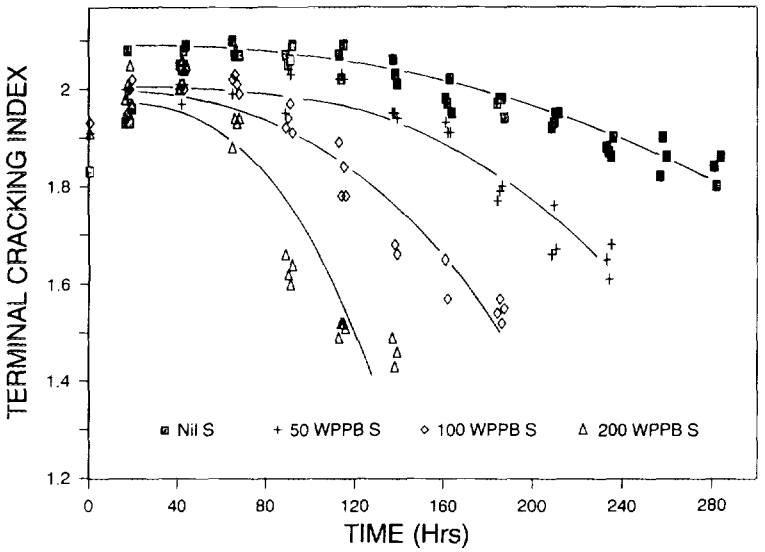

FIG. 6. Effect of feed sulfur content on the terminal cracking index of a 0.6% Pt/KL extrudate catalyst. Nil-sulfur feed contains no added sulfur; 50–200 wppb sulfur feeds obtained by thiophene addition.

about 10% (12–14 Pt atoms near the two KL entrances/130 total Pt atoms in channel) of the total available Pt sites are used to produce a double channel blockage.

Significant modification of the catalytic properties of Pt by the presence of chemisorbed sulfur can be ruled out by considering the benzene yield versus benzene selectivity plot presented in Fig. 8. The common curve shared by the nil-sulfur and three sulfur-added runs strongly suggests that sulfur-deactivation occurs by progressive loss of active Pt sites within the KL channels (resulting primarily from double channel blockage of Pt agglomerates) and not by altering the electronic nature of such sites. A common curve would not have been obtained if deactivation resulted from adsorbed sulfur

TABLE 1

Effect of Feed Sulfur Concentration on the Performance and Agglomeration of a Pt/KL Catalyst

Feed sulfur (wppb)[a]	Time on feed (hr)	Time (hr) to converge to 8 wt% benzene yield[b]	S/Pt (atom ratio)	Sulfur (wppm) on catalyst		Pt particle size (Å)[d]
				Found	Calculated	
nil	285	—	—	—	—	13
50	235	340	0.08	—	—	17
100	190	220	0.10	—	—	20
200	140	125	0.10	—	—	28
200[c]	330	275	0.09	95	118	—

[a] Sulfur added in the form of thiophene.

[b] Run conditions: 783 K, 6.6 WHSV, 825 kPa, hexane/methylcyclopentane feed and H_2/feed ratio of 6.

[c] Same conditions as footnote (*b*) except WHSV of 2.5 utilized.

[d] Predominant Pt particle size in recovered catalyst; determined by Z-contrast STEM measurements.

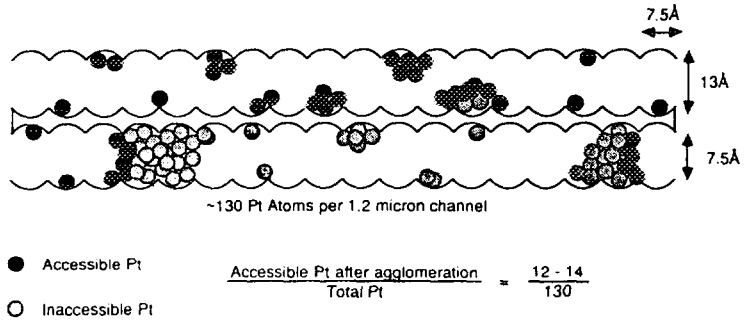

FIG. 7. Proposed model for pore mouth blockage of Pt/KL catalysts.

electronically modifying the activity and selectivity of exposed Pt surfaces. It should also be noted that extended hydrogen reduction of sulfur deactivated Pt/KL catalysts will not restore catalyst performance, even though such treatment removes substantial amounts of sulfur from the catalyst. This observation supports the suggestion that sulfur causes an irreversible reduction in the number of Pt sites accessible within the KL channels.

Infrared spectra of adsorbed CO are consistent with deactivation occurring by the systematic loss of accessible Pt sites, and not by electronic and/or geometric modification of Pt surfaces by adsorbed sulfur. Figure 9A shows the IR spectrum of reduced and outgased Pt/KL in equilibrium with 10 Torr of CO. In accord with a previous study of carbon monoxide on Pt in alkali-L zeolites (*26*), the spectrum of the fresh catalyst is dominated by a broad, structured peak centered near 2000 cm^{-1} (terminal CO) and also contains a weaker, broad feature near 1800 cm^{-1} (bridging CO). Spectra recorded at lower CO coverage (i.e., during CO TPR)

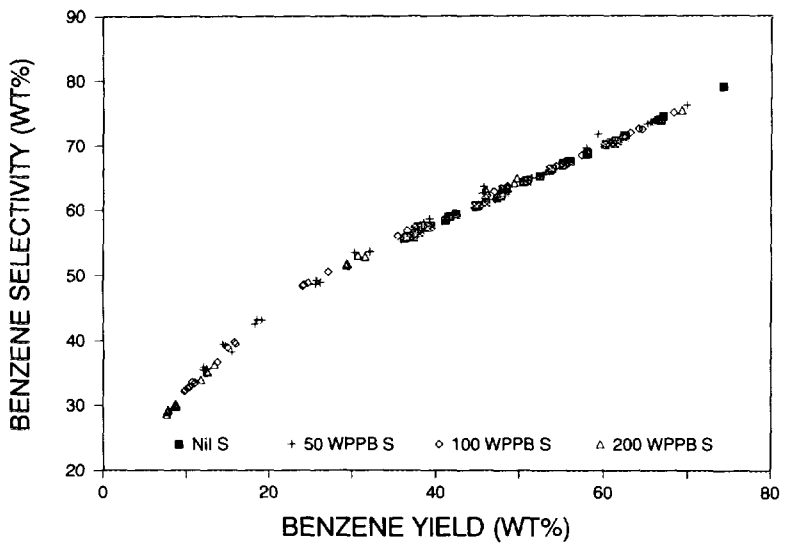

FIG. 8. Correlation between benzene yield and benzene selectivity for a 0.6% Pt/KL extrudate catalyst is independent of feed sulfur content. Nil-sulfur feed contains no added sulfur; 50–200 wppb sulfur feeds obtained by thiophene addition.

show a steady shift of these band manifolds to even lower frequencies. As others have noted, the spectrum is markedly different from that of carbon monoxide on alumina-, silica-, or titania-supported Pt (*27, 28*). On these macroporous supports the spectrum typically contains an intense, comparatively narrow terminal CO-band near 2080 cm^{-1} and a less intense bridging CO feature near 1840 cm^{-1}. The relatively low frequencies for CO on KL-supported Pt presumably reflect perturbations of CO–Pt bonds by the strongly basic environment within the KL channels. Spectral deconvolution suggests that the absorption bands are broad because they consist of overlapping features. A recent study identified at least five discrete terminal CO stretching frequencies on Pt/KL (*29*). This suggests the existence of an array of different K-Pt-CO binding interactions within the zeolite channels. Figure 9B shows the IR spectrum of CO on a partially deactivated Pt/KL sample recovered from a hexane aromatization run employing a 200-wppb sulfur feed. Relative to the fresh catalyst, the partially deactivated sample shows a 75% loss in integrated band intensity, but the band positions and shapes of both samples are similar. The spectrum is unaffected by subsequent calcination (673 K; O_2; 6 hr), rereduction, and exposure to CO, suggesting that the intensity attenuation is not due to coverage of Pt sites by coke. No new bands are seen on the sulfur-deactivated sample. Apestiguia, *et al.* have shown that coadsorbed sulfur increases the terminal CO stretching frequency on Pt/Al_2O_3 (*30*). By analogy we would expect the appearance of new higher frequency CO features if deactivation were primarily due to the presence of strongly bound sulfur (sulfur not removed by extensive reduction (H_2, 673 K) pretreatment of the IR sample.) Thus, the spectrum of the sulfur-deactivated catalyst (B) is most consistent with a reduction in the number of accessible carbon monoxide adsorption sites which likely arises from blockage of KL channels by Pt agglomerates.

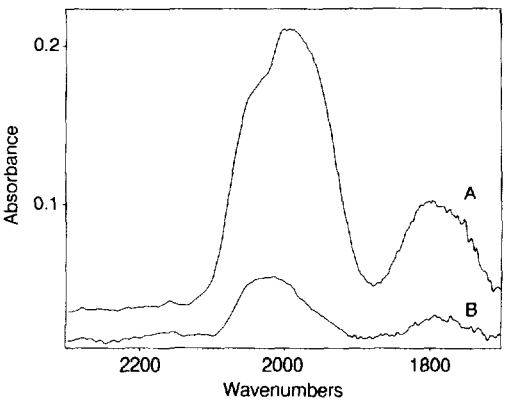

FIG. 9. Infrared spectra of a fresh (A) and sulfur-deactivated (B) 0.6% Pt/KL extrudate catalysts under 10 Torr CO following reduction and evacuation. Sulfur-deactivated sample (B) was recovered from a 200-wppb feed sulfur hexane aromatization experiment (see Experimental section for details).

Effect of Sulfur on the Size and Location of Pt Particles in Pt/KL Catalysts

In combination with the preceding and additional hexane aromatization tests, electron microscopy measurements were employed to enhance our understanding of the underlying factors responsible for the extreme sulfur sensitivity shown by Pt/KL catalysts. Figure 10 shows benzene yields obtained from three replicate experiments of different run lengths on an unbound 0.6% Pt/KL catalyst under accelerated deactivation test conditions of 793 K, 788 kPa, 50 WHSV, H_2/feed mole ratio of 6, and a nil-sulfur feed consisting of *n*-hexane (70%) and methylcyclopentane (30%). At run lengths of 1.5, 7.5, and 65 hr, the corresponding benzene yields were 56, 52, and 26 wt%, respectively. After 65 hr on feed about 1% carbonaceous material (i.e., coke) was found on the spent catalyst. Even in the presence of large quantities of methylcyclopentane (a notorious coke precursor), only small amounts of coke are generated on well prepared and activated Pt/KL catalysts, thus it is reasonable to assume that coke formation plays a relatively minor role during the initial stages of Pt/KL deactivation.

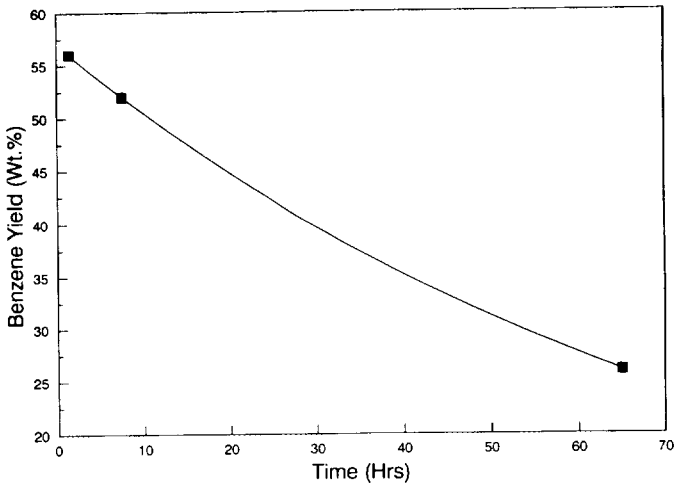

FIG. 10. Benzene yield as a function of time displayed by an unbound 0.6% Pt/KL catalyst under accelerated deactivation test conditions. A nil-sulfur feed was employed.

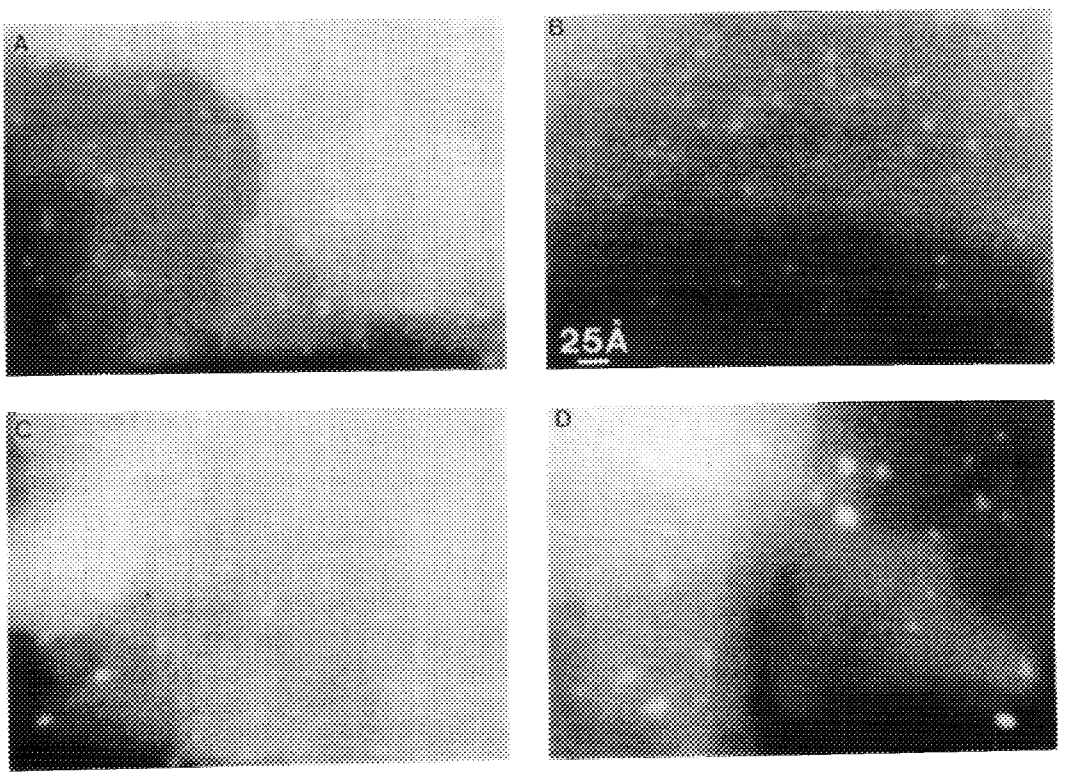

FIG. 11. *Z*-contrast STEM images of a fresh unbound 0.6% Pt/KL catalyst (A) and the same catalyst recovered from accelerated deactivation tests after 1.5 (B), 7.5 (C), and 65 (D) hr on a nil-sulfur feed. The white dots represent Pt clusters.

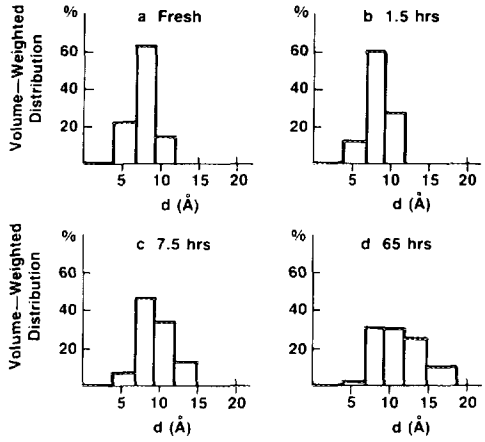

FIG. 12. Volume-weighted Pt particle size distributions of catalysts shown in Fig. 11. Histograms include those of a fresh unbound 0.6% Pt/KL catalyst (a) and the same catalyst recovered from accelerated deactivation tests after 1.5 (b), 7.5 (c), and 65 (d) hr on a nil-sulfur feed.

This assumption is strengthened by the observation that coked Pt/KL catalysts retain high H_2 adsorption uptakes (*24*), indicating thereby that coke is mainly associated with the KL support and not the Pt sites.

Catalysts recovered after 1.5, 7.5, and 65 hr on feed plus the fresh catalyst sample were examined by STEM. The *Z*-contrast images obtained using STEM are sensitive to the atomic number (*Z*), giving high contrast for high-*Z* particles such as Pt when supported on low-*Z* supports such as alumina, silica, and KL zeolites (*31*). The *Z*-contrast technique has generally been found to be more sensitive than conventional bright-field TEM imaging methods for detecting small Pt particles on KL (*19*). Figures 11 and 12 show representative STEM micrographs and volume-weighted particle size distributions, respectively, for Pt clusters in the above four catalyst samples. The histograms shown in Fig. 12 were constructed by measuring the diameters of at least 500 Pt particles in each of the four samples. The data in Fig. 12 are corrected for image broadening due to the finite width of the electron beam, which is estimated to be 4 Å. An experimental confirmation of this image broadening effect is based on the premise that upon agglomeration, Pt particle widths are limited by the zeolite L cage to a maximum diameter of about 13 Å. In the *Z*-contrast images the measured image widths of such agglomerated Pt clusters (measured from channel wall to channel wall) seldom exceed 17 Å. This was assumed to translate into 13 Å actual diameter.

In the fresh unbound Pt/KL catalyst, the majority of the Pt(>85%) is present as sub-10-Å clusters within the KL channels. With increasing time on feed, particle sizes coarsen with an accompanying buildup in the number of Pt clusters exceeding 13 Å in diameter. The average volume-weighted Pt particle sizes are 6.7, 8.1, 8.8, and 9.8 Å, respectively, for the fresh, 1.5, 7.5, and 65 hr on nil-sulfur feed catalyst samples. It should be noted that this unbound catalyst is an experimental catalyst from early development efforts. The procedure used to prepare this particular catalyst was not optimized. In principle, if the zeolite structure were rigid, cluster diameters could not exceed the 13-Å channel width. However, clusters are free to grow along the channel direction, thereby forming elongated particles. Electron microscopy evidence for extended Pt cluster growth in the direction of the KL channel is often observed in Pt/KL catalysts recovered from long term, high temperature hexane aromatization experiments. The bright-field TEM micrograph shown in Fig. 13 clearly shows the presence of Pt clusters aligned with the KL channels.

After extended times on feed Pt particles begin to accumulate outside the channels either by diffusion of Pt atoms or by particle migration. Without the constraint of the KL cage, Pt can grow to much larger crystallite sizes. Based on the histogram in Figure 12d, an upper limit for the amount of external Pt clusters after 65 hr on oil is estimated to be about 15%. As shown in Fig. 10, over the 65 hr run length benzene yields decreased about 50%. The smooth decline in aromati-

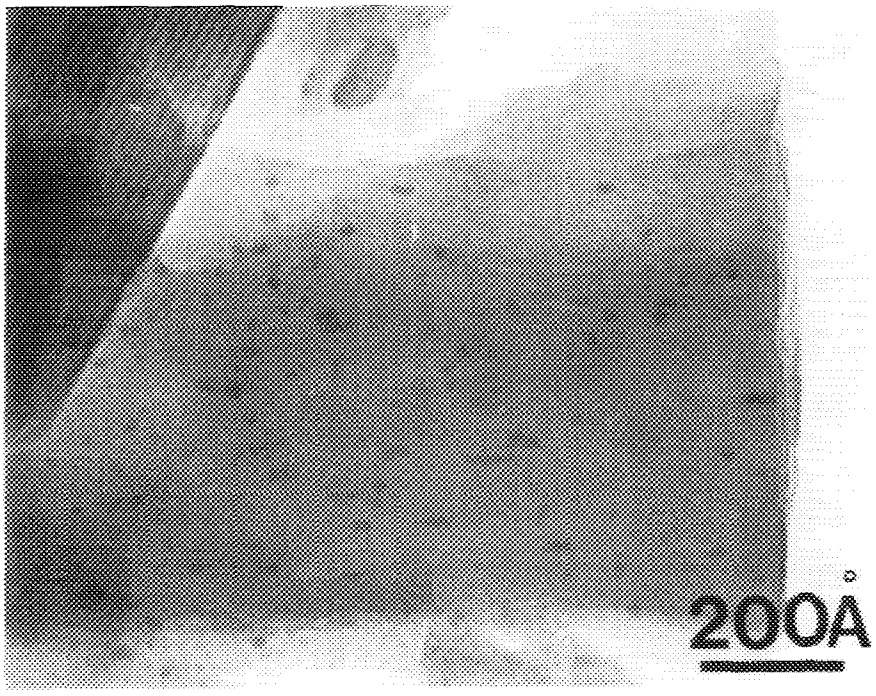

FIG. 13. Bright-field TEM micrograph of an unbound 0.6% Pt/KL catalyst showing the presence of Pt clusters elongated along the KL channel. The catalyst was recovered from an aromatization experiment after 100 hr on a feed containing 50 wppm sulfur. KL-zeolite channel spacings of 15.9 Å are visible and provide an internal standard for Pt cluster size measurement.

zation activity most likely results from the slow but continuous growth of 7–13 Å Pt particles within the KL channels reducing, thereby, the number of Pt sites which can be accessed by hexane molecules.

The observation (see Table 1) that 17 to 28 Å Pt clusters are generated in the presence of 50 to 200 wppb sulfur feed concentrations (13 Å Pt clusters in the absence of added sulfur) strongly indicates that sulfur accelerates Pt agglomeration. Thus, the extreme sulfur sensitivity exhibited by Pt/KL catalysts results, in large part, from KL channel blockage by Pt particles upon which sulfur may or may not be chemisorbed. The use of higher feed sulfur concentrations (280 wppb sulfur) resulted in the formation of elongated Pt (20–50 Å) crystallites situated just inside the KL channels, near the pore mouth basal planes (see Fig. 14). The observation that Pt agglomerates tend to form at the KL channel entrance supports the contention that deactivation, at least in the initial stages, occurs by pore mouth plugging of KL channels by 10–20 Å Pt and/or Pt–sulfur particles.

SUMMARY

For initially well-dispersed Pt/KL catalysts, with little or no Pt outside of the zeolite channels, Pt agglomeration is a primary deactivation mechanism. The role of agglomeration is presumably to create multiple blockages within the one-dimensional KL channels, thereby entombing active Pt sites. Sulfur present at the wppb level in the feed accelerates Pt agglomeration and thereby increases catalyst deactivation. Sulfur, however, does not appear to modify the intrinsic catalytic properties of accessible platinum sites within the channels of KL zeolites.

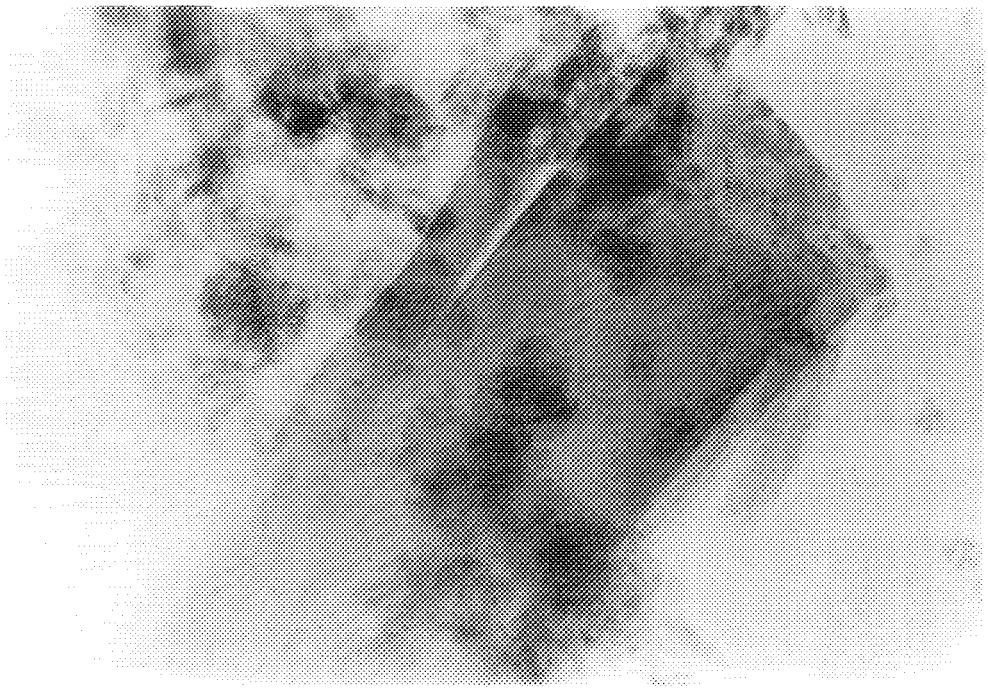

FIG. 14. Bright-field TEM micrographs of a sulfur-deactivated 0.6% Pt/KL extrudate catalyst deactivated under a 280-wppb sulfur feed. KL-zeolite channel spacings of 15.9 Å are visible and provide an internal standard for Pt cluster size measurement. Note that platinum particles have agglomerated and are clustered predominantly toward the basal plane (channel entrance) of the KL crystallite.

REFERENCES

1. Bernard, J. R., *in* "Proceedings, 5th International Zeolite Conference" (L. V. Rees, Ed.), p. 686. Heyden, London, 1980.
2. Hughes, T. R., Jacobson, R. L., and Tamm, P. W., *in* "Catalysis 1987" (J. W. Ward, Ed.), p. 317. Elsevier, Amsterdam, 1988.
3. Tamm, P. W., Mohr, D. H., and Wilson, C. R., *in* "Catalysis 1987" (J. W. Ward, Ed.), p. 335. Elsevier, Amsterdam, 1988.
4. Law, D. V., Tamm, P. W., and Detz, C. M., *Energy Process* **7**, 215 (1987).
5. Breck, D. W., U.S. Patent 3,216,789 (1965).
6. Wortel, T. M., U.S. Patent 4,544,539 (1985).
7. Poeppelmeier, K. R., Funk, W. G., Steger, J. J., Fung, S. C., Cross, V. R., and Kao, J. L., U.S. Patent 4,959,668 (1986).
8. Tauster, S. J., Montagna, A. A., Steger, J. J., Fung, S. C., and Cross, V. R., U.S. Patent 4,595,670 (1986).
9. Fung, S. C., and Tauster, S. J., U.S. Patent 4,595,669 (1986).
10. Fung, S. C., Tauster, S. J., and Koo, J. Y., U.S. Patent 4,925,819 (1990).
11. Hughes, T. R., Buss, W. C., Tamm, P. W., and Jacobson, R. L., *in* "Proceedings, 7th International Conference" (Y. Murakami, A. Lijima, and J. W. Ward, Eds.), p. 725. Kodansha, Tokyo, 1986.
12. Besoukhanova, C., Breysse, M., Bernard, J. R., and Barthomeuf, D., *in* "Catalyst Deactivation" (B. Delmon and G. F. Froment, Eds.), p. 201. Elsevier, Amsterdam, 1980.
13. Buss, W. C., Field, L. A., and Robinson, R. C., U.S. Patent 4,456,527 (1984).
14. Poeppelmeier, K. R., Trowbridge, T. D., and Kao, J. L., U.S. Patent 4,568,656 (1986).
15. Sinfelt, J. H., Carter, J. L., and Yates, D. J. C., *J. Catal.* **24**, 283 (1972).
16. Spenadel, L., and Boudart, M., *J. Chem. Phys.* **64**, 204 (1960).
17. Sulfur analyses were performed by the Analytical Science Laboratory, Exxon Research and Engineering Company, Annandale, NJ.
18. Rice, S. B., and Treacy, M. M. J., *in* "Specimen Preparation for Transmission Electron Microscopy

of Materials" (J. C. Bravman, M. L., McDonald and R. Anderson, Eds.), Materials Research Society Symposium Proceedings, Vol., 115, p. 15. Mater. Res. Soc., Pittsburgh, PA, 1988.
19. Rice, S. B., Koo, J. Y., Disko, M. M., and Treacy, M. M. J., *Ultramicrosc.* **34,** 108 (1990).
20. Robbins, J. L., *J. Catal.* **115,** 120 (1989).
21. Tauster, S. J., and Steger, J. J., *J. Catal.* **125,** 387 (1990).
22. Derouane, E. C., and Vanderveken, D. J., *Appl. Catal.* **45,** L15 (1988).
23. Tauster, S. J., and Steger, J. J., *Mater. Rec. Soc. Symp. Proc.* **111,** 419 (1988).
24. Iglesia, E., and Baumgartner, J. E., *in* "Preprints, 10th International Congress on Catalysis, Budapest, 1992," p. 157. Institute of Isotopes of the Hungarian Academy of Sciences, Budapest, 1992.
25. Larsen, G., and Haller, G. L., *Catal. Lett.* **3,** 103 (1989).
26. Besoukhanova, C., Guidot, J., Barthomeuf, D., Breysse, M., and Bernard, J. R., *J. Chem. Soc. Faraday Trans. 1* **77,** 1595 (1981).
27. Sheppard, N., and Nguyen, T. T., *In* "Advances in Infrared and Raman Spectroscopy" (R. J. Clark and R. E. Hester, Eds.), Vol. 5, p. 67. Heyden, London, 1978.
28. Robbins, J. L., and Marucchi-Soos, E., *J. Phys. Chem.* **91,** 2026 (1987).
29. Kustov, L. M., Ostgard, D., and Sachtler, W. M. H., *Catal. Lett.* **9,** 121 (1991).
30. Apesteguia, C. R., Brema, C. E., Garetto, T. F., Borgna, A., and Parera, J.M., *J. Catal.* **89,** 52 (1984).
31. Treacy, M. M. J., and Rice, S. B., *J. Microsc.* **156,** 211 (1989).